Atmospheric Research 100 (2011) 603–620

Contents lists available at ScienceDirect

Atmospheric Research

journal homepage: www.elsevier.com/locate/atmos

Initiation of a severe thunderstorm over the Mediterranean Sea

J.B. Cohuet [a,*], R. Romero [b], V. Homar [b], V. Ducrocq [a], C. Ramis [b]

[a] GAME-CNRM, Météo-France and CNRS, 42 av. Gaspard Coriolis, 31057, Toulouse, France
[b] Departament de Física, Universitat de las Illes Balears, Carretera de Valldemosa km 7.5, 07122, Palma de Mallorca, Spain

ARTICLE INFO

Article history:
Received 14 February 2010
Received in revised form 31 October 2010
Accepted 1 November 2010

Keywords:
Mediterranean convection
Bow echo
Mesovortices

ABSTRACT

The Mediterranean basin is regularly affected by severe weather associated with deep convection. Although convective systems are usually linked to coastal orography, some severe thunderstorms develop and mature over the sea. A recent example is the severe thunderstorm that affected the island of Mallorca in the afternoon of 4 October 2007. The storm formed early in the morning offshore of Murcia, and steadily became organized into a squall line. Arriving in Palma city, this squall line produced severe gusts, heavy rain and several tornadoes. The initiation and evolution of convection in these kinds of maritime events depend on both synoptic and mesoscale features. Representing such interactions is a challenge for numerical weather prediction. The aim of this study is to determine the prominent factors involved in the initiation and evolution of the damaging squall line, by means of high resolution numerical experiments. We also focus on squall line mesovortices to explain the potential for tornado development and the role of Mallorcan orography on their evolution.

Simulations performed with the mesoscale model Méso-NH allowed relevant mechanisms for initiation and development of the strong squall line to be identified. The squall line initiates in an area with conditional instability, characterized by a cut-off and a southerly jet aloft and by moist, warm air at low-levels along a front. In addition, the area of low-level convergence offshore of Murcia, associated with the front and enhanced by a low downstream of the Atlas range, was shown to be crucial during the early stage of the convective system. The dry layer in the mid-troposphere and the strong sheared environment provide elements for understanding the development of such a damaging squall line. Moreover, a very high resolution experiment (600 m mesh) gave a very realistic representation of the squall line, including mesovortices ahead of the gust front, which confirmed the potential of this strong convective system for the genesis of small-scale vortices that may precede tornado development. A sensitivity experiment pointed out the prominent role of Mallorcan orography in straightening mesovortices approaching Palma city, and provided interesting elements for the understanding of the localization of tornadoes that occurred on 4 October 2007.

1. Introduction

Deep convection develops fairly frequently in all countries surrounding the Mediterranean basin. In particular, these densely populated areas have seen catastrophic flash-flood events often characterized by quasi stationary systems like those of Vaison-la-Romaine in southern France on 22 September 1992 (Sénési et al., 1996), Gandia in Central Valencia on 3 November 1987 where more than 800 mm of precipitation was recorded in 24 h (Llasat and Puigcerver, 1994) or like the catastrophic floods of the Piedmont region in northwestern Italy on 5 November 1994 (Buzzi et al., 1998; Doswell et al., 1998). Reports of these events demonstrate that the role played by the orography both in forcing mesoscale circulations and producing direct uplift to moist surface air parcels is fundamental for the initiation and the

* Corresponding author. Present affiliation: Météo-France, DSO/DOS/OCE 42 av. G. Coriolis, 31057 Toulouse, France.
E-mail address: jean-baptiste.cohuet@meteo.fr (J.B. Cohuet).

0169-8095/$ – see front matter © 2010 Elsevier B.V. All rights reserved.
doi:10.1016/j.atmosres.2010.11.002

maintenance of such thunderstorms. However, some Mediterranean severe thunderstorms develop and mature over the sea, without direct orographic forcing (Homar et al., 1999). These mesoscale convective systems may also reach the coastlands and affect populated areas.

A recent example of this kind of convection was the severe thunderstorm that swept across the island of Mallorca (Fig. 1) on the afternoon of 4 October 2007. Initiated early in the morning offshore of Murcia, this storm progressively became organized into a squall line as it moved northeastwards. When the system arrived over Palma, it produced severe gusts, heavy rain and even several tornadoes. Palma suffered unprecedented traffic disruption due to exceptional rain and wind intensities. Winds tore down hundreds of trees, traffic signs and lights, affecting road connections in the centre and north of the island. Some streets of Palma were flooded with more than 50 cm of water in places. This storm injured 200 people and even killed one person. It caused significant damage in the southwestern part of the island and economic losses were estimated at several tens of millions of Euros (Ramis et al., 2009).

Representing the initiation, organization and evolution of convection within these maritime events is a challenge for numerical weather prediction models, which have to capture both synoptic and mesoscale features. Western coastal Mediterranean regions are known to be particularly favourable to the development of Mesoscale Convective Systems (MCS) often linked with heavy rainfall events and especially frequent under specific weather regimes. Several studies have underlined the conditions that most frequently lead to these phenomena: on the one hand, a strong humid low-level flow coming from the sea and, on the other hand, a large-scale trough over France and Spain associated with a southwesterly diffluent jet streak aloft (Romero et al., 1999; Nuissier et al., in press). In addition, upper-level precursors such as upper-level Potential Vorticity (PV) streamers or a deep short trough are often put forward to explain convection initiation (Fehlmann et al., 2000; Massacand et al., 1998; Homar and Stensrud, 2004). It is frequent that MCS develop over the Alboran Sea or to the south of the Balearic Islands during the autumn, as the sea is quite warm after the high insolation throughout the summer (Riosalido, 1990). Mesoscale ingredients necessary to initiate and sustain Mediterranean convection have been extensively analysed in the past by means of numerical models. In particular, the orography plays a crucial role when a moist and conditionally unstable low-level jet impinges on coastal mountains (Romero et al., 2000; Scheidereit and Schär, 2000; Ducrocq et al., 2008). The deep convection itself can have an influence on the initiation and evolution of the convection. The prevailing role of convectively induced cold pools has been demonstrated to explain the propagation of convective systems over the Mediterranean Sea (Romero et al., 2001; Ducrocq et al., 2008) as over land (Khairoutdinov and Randall, 2006, among others) or in maintaining the system upstream of the mountains (Bresson et al., 2009).

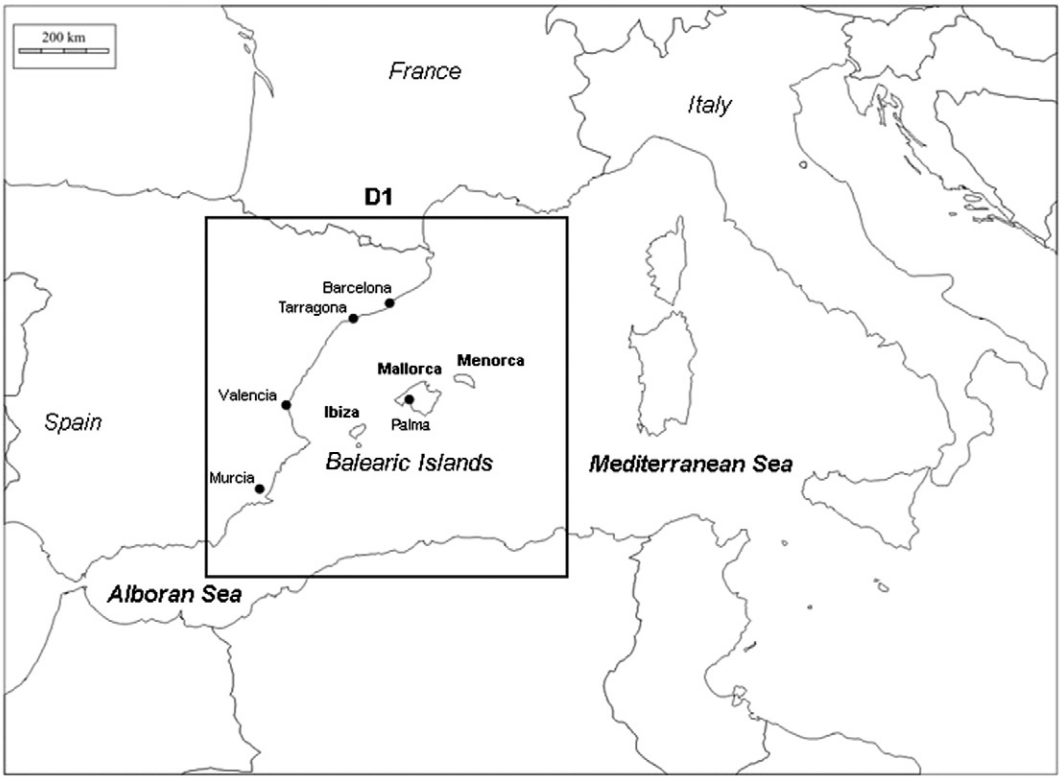

Fig. 1. Geographic references and domain D_1 used for $MNH_{2.4}$ simulation.

On 4 October 2007, the presence of at least one F2 tornado was related with a short length maritime squall line apparently devoid of supercells (Ramis et al., 2009). Mechanisms for tornadogenesis are generally classified in two categories (Trapp and Davies-Jones, 1997). The genesis of type I tornadoes is linked with supercell dynamics and can lead to very powerful tornadoes. Although this kind of formation prevails, tornadoes are also observed in quasi-linear convective systems (QLCS). These tornadoes (type II) are known to be weaker and shorter-lived on average than those associated with supercells (Houze, 1993). However, this second type of genesis should not be neglected. Observational studies by Tessendorf and Trapp (2000) and Trapp et al. (2005) show that it represents 20% of tornadic events in the United States. QLCS tornadoes occur in convective lines without supercells (the most frequently) as well as in supercells embedded in convective lines.

Numerical studies (Weisman and Trapp, 2003; Trapp and Weisman, 2003) have demonstrated that the genesis of type II tornadoes is linked with an intensification of low-level mesovortices as in supercell tornadoes. These low-level mesovortices have typical diameters of a few kilometres. Mesovortex genesis is initiated at low-levels by the tilting of baroclinically generated horizontal vorticity. In mature QLCS, such horizontal vorticity located just rearward of the gust front is the consequence of the strong thermal gradient separating the cold pool from the surrounding environment. Later, the intensity of the vertical low-level mesovortex grows by vertical stretching. Mesovortex strength depends upon several factors: the environmental shear, the Coriolis forcing, and the cold pool magnitude. According to Weisman and Trapp (2003), the Coriolis force has a direct impact on the enhancement of low-level cyclonic mesovortices and also on the decline of anticyclonic mesovortices. However, not all cyclonic mesovortices produce tornadoes, which form with a sudden increase of low-level vorticity. This process remains incompletely understood at present. A plausible explanation often proposed is the transport of vorticity from the atmospheric layer between 1 and 3 km to the surface by strong downdrafts.

The theory commonly mentioned to explain the tilting of horizontal mesovortices to the vertical in QLCS is described in Trapp and Weisman (2003). They consider that, unlike supercell cases where mechanisms leading to the vertical vorticity tilting are ascribable to updrafts, in bow echoes, this role is played by downdrafts at the leading edge of the cold pool. Other studies endorse this downdraft theory (Wakimoto et al., 2006; Wheatley and Trapp, 2008), identifying precipitation-induced downdrafts as the mechanism to tilt horizontal vorticity. However, the recent investigations of Atkins and St. Laurent (2009b) lead to the conclusion that there may be other processes that can also produce mesovortices within bow echoes. Based on quasi-idealized numerical simulations, they found that a localized updraft produced upward tilting of cold pool vortex lines, resulting in the genesis of vertical mesovortex couplets. Such mesovortex couplets seem to appear in the early stages of the

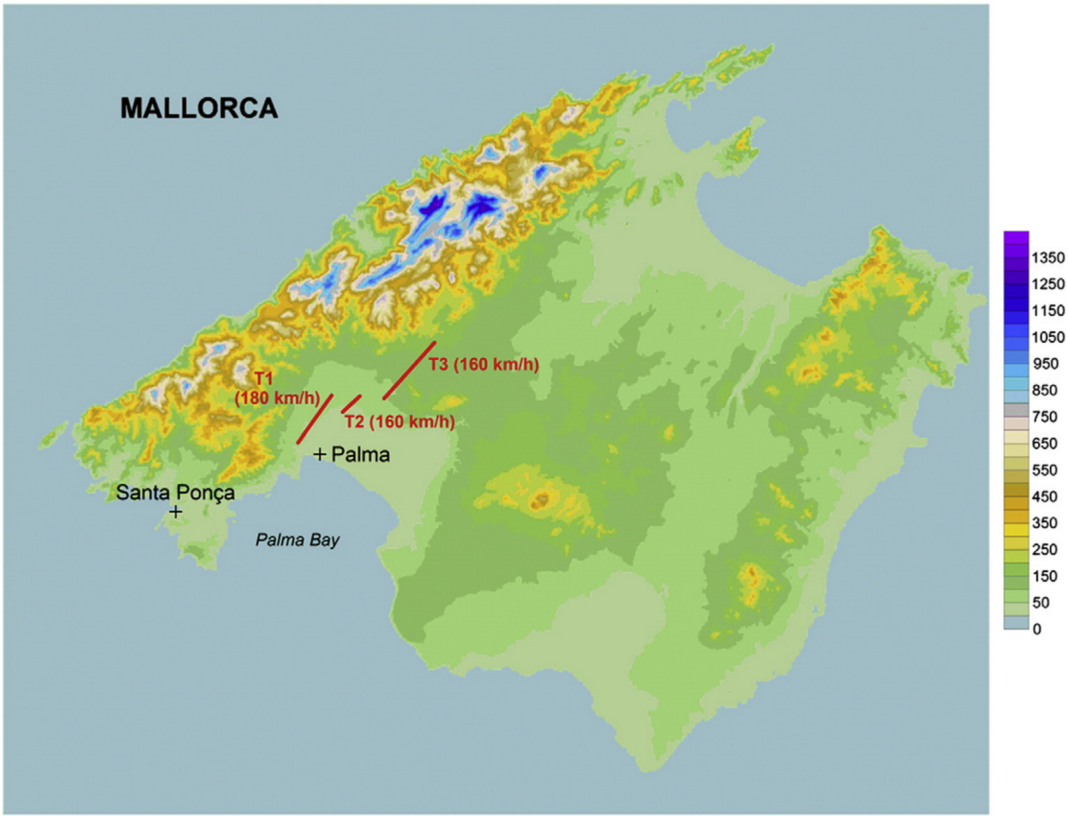

Fig. 2. Mallorcan orography (shaded, m), tornado locations and maximum wind intensity according to AEMET damage study.

bow echo life cycle. The authors also document the genesis of single cyclonic mesovortices which, in contrast, affects all the stages of the bow echo life cycle.

A major aim of this study is to confirm the tornado genesis type (QLCS non-supercell tornadoes) for the 4 October 2007 real case and to study the genesis of mesovortices, based on high-resolution simulations. Simulating the maritime convective system with an organization close to that observed was a prerequisite for this study and led us to test several models and initial conditions. Only the best simulation is discussed here. The influence of Mallorcan orography on mesovortices is also discussed.

This paper is organized as follows. The next section analyses the observations available for the case. Then, Section 3 presents the numerical experiment used to simulate the squall line. This is followed, in Section 4, by the analysis of the simulated squall line in order to investigate its generation and the environment favourable for tornadogenesis.

2. The case study

2.1. Ground observations

In the afternoon of 4 October 2007, a squall line entered the island of Mallorca from the southwest and moved northeastwards at a speed of about 80 km h^{-1}, accompanied by violent winds and torrential rain. The damage analysis made by AEMET (Agencia Estatal de Meteorologia, Spanish Meteorological Institute) proves the presence of at least one F2 tornado embedded in the system (T1 in Fig. 2). Associated winds were estimated at 180 km h^{-1}, for the maximum intensity, and the tornado path width reached 200 m in places. Two other tornadoes were identified from the damage caused, with a maximum intensity reaching 160 km h^{-1} and a width assessed to be 100 m. The city of Palma de Mallorca and especially its industrial suburbs to the north, were the most affected areas, with huge damage being reported.

Before arriving over Mallorca, the squall line affected Ibiza at 1400 UTC, where gusts reached 80 km h^{-1}. One hour later, the system was progressing toward Mallorca Island, affecting Palma bay. Data recorded in Mallorca during the afternoon indicate that more than 40 mm of rain fell during this severe event. The observatory of Palma recorded gusts reaching 109 km h^{-1} and the rain gauge measured 18 mm in only 10 min (data not shown). Furthermore, this storm produced small hailstones. The electric activity was also exceptional. The LINET lightning detection network (Betz et al., 2009) recorded 160 lightning strikes over the island in only 10 min (Fig. 3).

The temperature graph in Fig. 4a of Santa Ponça, a city near Palma, shows a fall of 8° with the passage of the MCS, which began 1 h before the rain due to pre-squall clouds shrouding the sky, and which deepened sharply later, as a consequence of rain

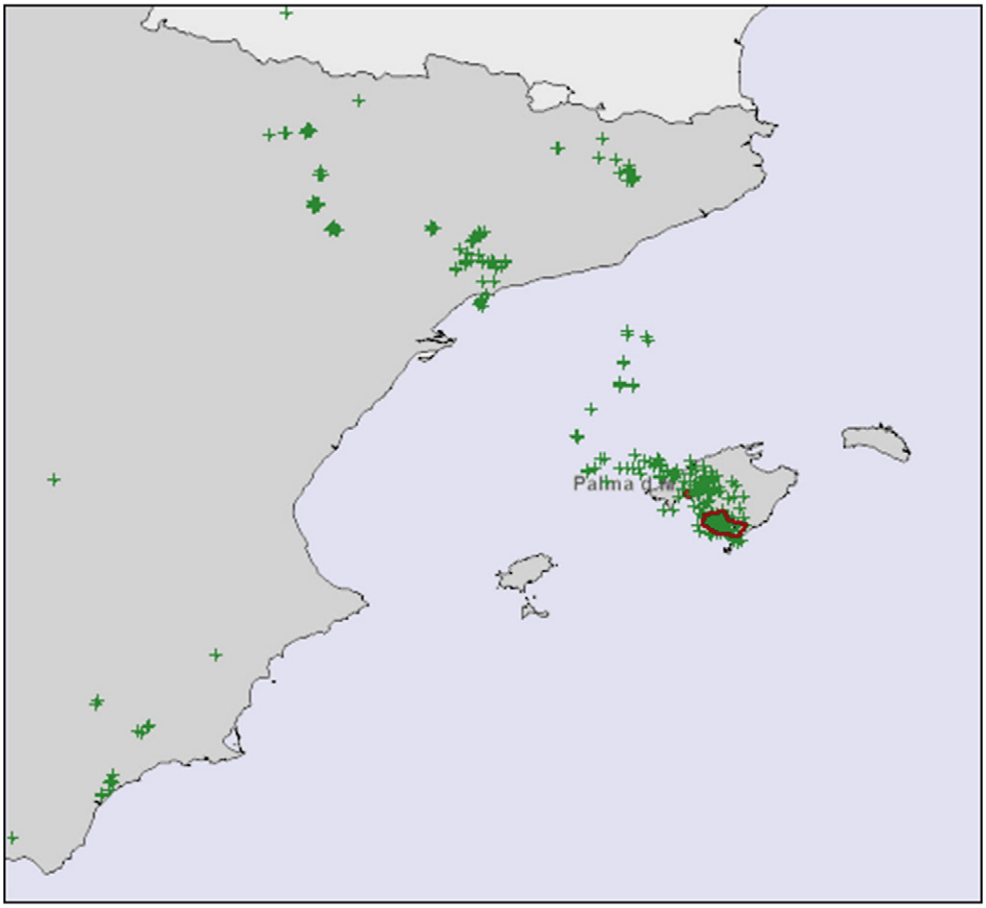

Fig. 3. Lightning strikes on 4 October 2007 from 1540 UTC to 1550UTC (LINET network).

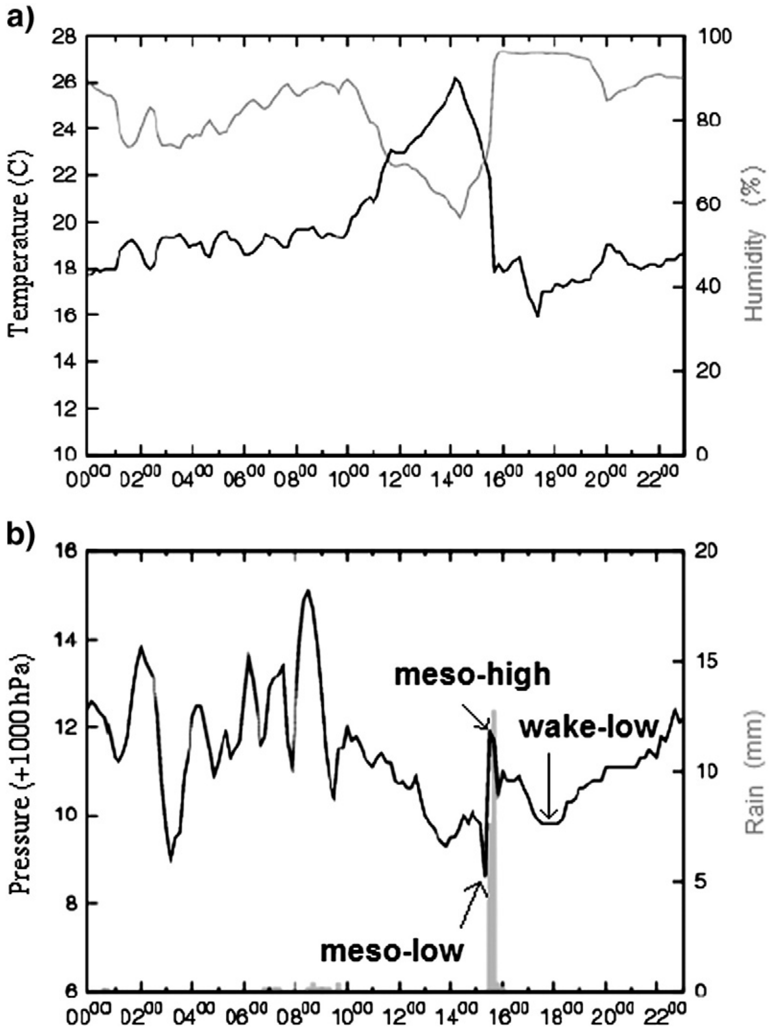

Fig. 4. Time-series observed at the Santa Ponça weather station (west of Mallorca) on 4 October 2007: (a) temperature and relative humidity, and (b) pressure and rainfall.

evaporation when the storm arrived. The pressure evolution during this day at Santa Ponça (Fig. 4b), as at other Balearic weather stations, shows the signature of a pre-squall meso-low just before the arrival of heavy rain, followed by a meso-high and then a wake low when the squall line was moving away. This kind of evolution matches what has been described in previous cases of observed squall lines (Johnson, 2001) and in particular in the western Mediterranean (Ramis et al., 1999). Such large pressure oscillations have been associated with large-amplitude gravity waves responsible for atmospherically forced seiches in bays and harbours of the Balearic Islands, which were particularly enhanced at Ciutadella harbour in Menorca (Ramis and Jansa, 1983; Montserrat et al., 1991). In addition, the rainfall registered in Santa Ponça indicates the brevity and the intensity of rain associated with the squall line.

2.2. Radar and satellite data

Data from satellites and radars give more information about this storm, which started offshore of Murcia, at 0600 UTC. It is noteworthy that, during the night and the morning, two previous MCS evolved northeastwards over the sea (MCS1 and MCS2 in Fig. 5). After the initiation of the third MCS, the thunderstorm stayed almost stationary from 0700 to 1000 UTC. From the infrared and the High Resolution Visible (HRV) images (Figs. 5 and 6a) a V-shaped structure of the thunderstorm can be assumed with an overshooting top and a warm spot just to the north. Later, the system MCS3 began to progress slowly eastwards for 2 h and then started moving faster to the northeast while a linear structure was forming in its southern part. Although it was located at the limit of the radar of Valencia, it can be inferred from lightning strikes that the squall line of about 60 km length had its maximum strike rate approaching the bay of Palma at 1500 UTC. In the time sequence shown in Fig. 7, the progressive transformation of the system MCS3 into a squall line is clearly visible. At this time, the overshooting cloud tops were impressive, reaching heights of 16 km, a very unusual feature at these latitudes (Fig. 6b). Associated with this squall line, a widespread stratiform part further west shrouded the Balearic channel.

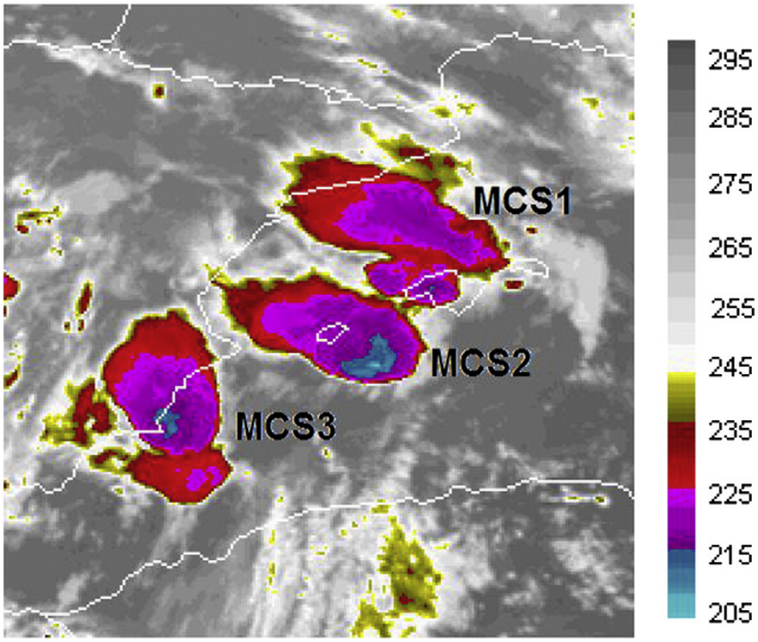

Fig. 5. Meteosat IR images at 0800 UTC 4 October 2007, with cloud top temperatures (K).

2.3. Analysis of synoptic patterns

In the upper levels, the synoptic situation was characterized by an upper-level trough over mainland Spain associated with cold air aloft, which promoted the potential instability as shown by the ARPEGE analysis at 1200 UTC (Fig. 8a). Geopotential height and temperature at 500 hPa indicate a low centred over mainland Spain and also affecting the Alboran Sea. This cut-off enhanced a southwesterly flow at mid- and upper-tropospheric levels which resulted in a diffluent jet aloft stretching from North Africa to the Balearic Islands, making the environment propitious for synoptic lifting. The synoptic scenario at low-levels was dominated by a low centred over the Sahara in the morning, which later moved towards the Balearic archipelago along the edge of the upper-level cut-off low. This low pressure area induced an easterly flow over the southern Mediterranean Sea. Also, a strong baroclinic boundary along the Spanish coast separated a tongue of African warm air, located over the sea, from drier and colder air over Spain (Fig. 8b). This thermal boundary was associated with a low-level wind convergence line and was characterized by a strong advection of moisture. The ARPEGE or ECMWF analyses (not shown) indicate that the front structure looked like a katafront, with a dry layer at mid-levels above the western part of the warm tongue.

Therefore, the synoptic environment was characterized by a well defined vorticity advection at 500 hPa that favoured upward motions over the western Mediterranean. Moreover, as usual in early autumn, sea surface temperature was high in this area, as testified by the 23 °C measured by several ships offshore of the Balearic Islands. Thus, it favoured evaporation, which supplied moisture to the low-levels as well as increasing the convective instability, as is often observed for Mediterranean heavy precipitating events (Lebeaupin et al., 2006). As a consequence of these patterns at low-levels and at upper-levels, the instability was pronounced at 0600 UTC over the western Mediterranean Sea, as shown by the CAPE on ARPEGE analysis presented in Fig. 9. The east of the Alboran Sea was the area most favourable to convective development with CAPE near to 1000 J kg^{-1} already present at 0600 UTC.

The sounding of Murcia at 0000 UTC (Fig. 10a), close to the thunderstorm onset location, gives an idea of the pre-convective environment. The temperature profile was weakly unstable (CAPE of about 62 J kg^{-1}) at this time for an air parcel near the ground. Note, however, that the CAPE value may have been higher offshore of Murcia, as surface cooling during the night is weaker over the sea. In addition, with this kind of sounding, the increase of the ground temperature after sunrise leads to a rapid rise of the CAPE. The layer between 600 and 450 hPa was quite dry, and this feature was important for enhancing the evaporation of descending gusts in MCS. The unidirectional shear below 700 hPa was noteworthy and in favour of a multicellular structure of the thunderstorm.

The analysis of the sounding of Palma at 1200 UTC (Fig. 10b) reveals some interesting features that help to explain the squall line organization. Even though the instability was not very pronounced at this time with a CAPE of 38 J kg^{-1} for a ground parcel, a dry layer between 950 and 700 hPa resulted in the creation of substantial convective inhibition energy (CIN = 355 J kg^{-1}) at low-levels. However, the updrafts associated with the squall line were able to break this layer and, above it, the sounding indicates that the environment was favourable to upward motions, with a high elevated CAPE. In addition, a strong southwesterly shear of about 20 m s^{-1} in the first three kilometres of the troposphere was also present over this area.

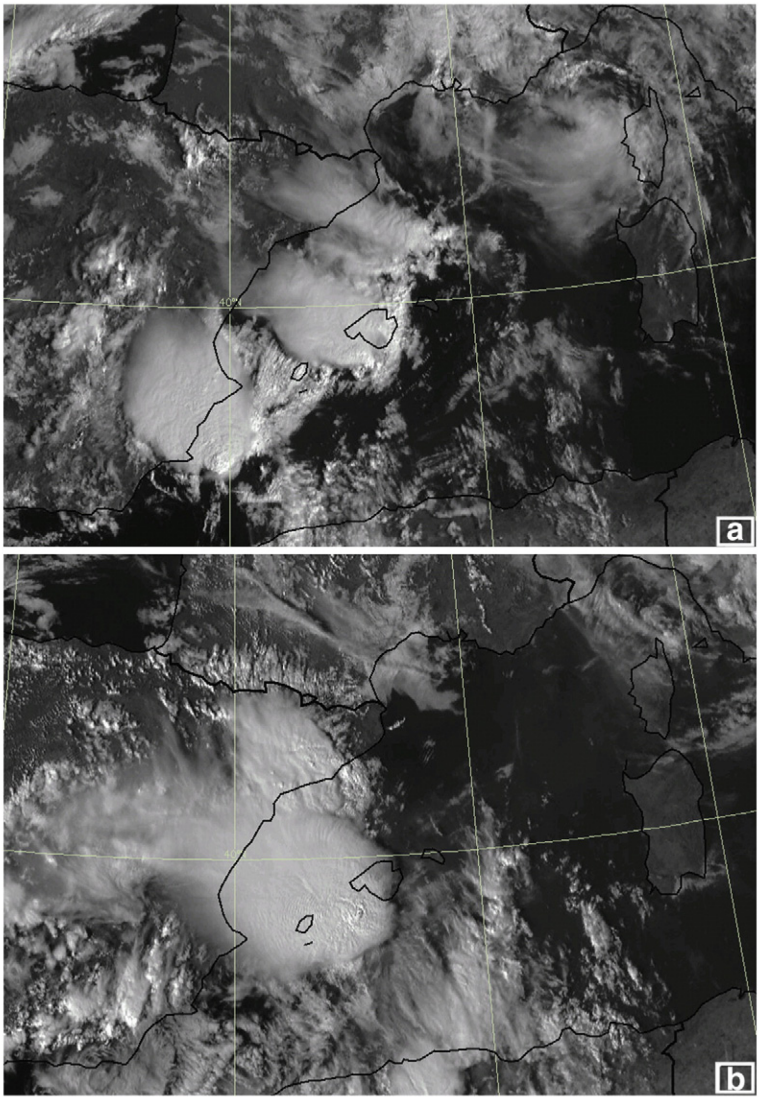

Fig. 6. Meteosat HRV images at (a) 0915 UTC and (b) 1500 UTC on 4 October 2007.

2.4. Summary of meteorological conditions favourable to the squall line formation

On 4 October 2007, several specific meteorological patterns were favourable to deep convection and others were indicative of a squall line organization. First, at low-levels, a thermal boundary was stretching over the western Mediterranean with a strong warm and moist easterly advection. At mid-levels, a low was centred over Spain, inducing a southwesterly diffluent flow over the same area, which was associated with a strong PV anomaly. The dry layer capping the warm one was also a crucial element in enhancing deep convection since it increased the rainfall evaporation rate and therefore the cooling responsible for stronger downdrafts. In spite of the fact that there was a strong inversion at low-levels, in the Balearic Islands area, some elements were able to release instability by breaking the dry layer. First an upper-level trough was moving northeastwards in the morning along the baroclinic area, producing synoptic lifting. Then, the front was characterized by a convergence of low-level winds. Next, the presence of earlier deep convection may have led to perturbed areas of surface pressure and winds. Although it is intricate to identify which one of these factors prevailed, their combination may have enabled more efficient triggering.

Although it is usually difficult to distinguish development of a squall line from development of an isolated storm, here some clues indicate a strong likelihood of preferentially finding this kind of structure among other MCS. First, the presence of a front seems to be favourable to squall line development ahead of it. In addition, the strong shear of horizontal wind present along the coastal area is a crucial pattern for the development of large, strong cells in the squall line (Bryan et al., 2005).

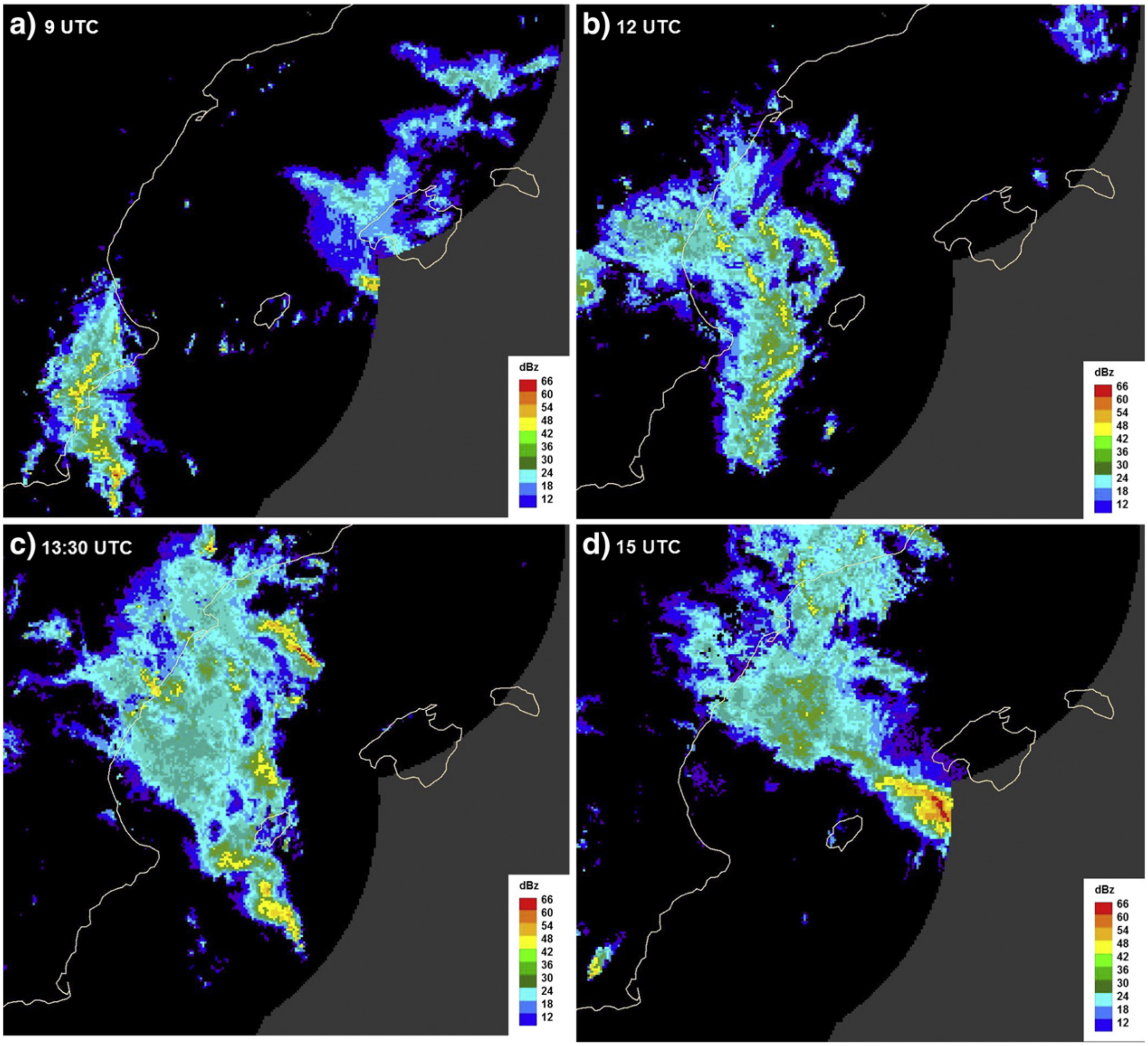

Fig. 7. Reflectivity composites from the Murcia, Valencia and Barcelona weather radar at 0900 UTC, 1200 UTC, 1330 UTC and 1500 UTC on 4 October 2007.

3. Characteristics of the numerical experiment

The simulation was performed with the research model Méso-NH at fine resolution to test its ability to capture the squall line event of 4 October 2007. Méso-NH is a 3D non-hydrostatic model (Lafore et al., 1998) in which the prognostic variables are the three dimensional wind components, the potential temperature, the turbulent kinetic energy, the mixing ratio of vapour and of five hydrometeor classes. Its temporal scheme is hybrid using a 4th order, centred scheme for momentum and a Piecewise Parabolic Method advection scheme (Colella and Woodward, 1984) for scalar variables. The microphysical parameterization (Pinty and Jabouille, 1998) is a bulk scheme based on Caniaux et al. (1994) for the evolution of the three ice categories (primary ice, snow and graupel) combined with a Kessler scheme for warm processes separating cloud water from rainwater. For horizontal resolution higher than 4 km, no deep convection parameterization is used. The turbulence parameterization is based on a 1.5 order closure (Cuxart et al., 2000) with the Bougeault and Lacarrère mixing length (1989).

The model configuration used here had been proved suitable for simulating Mediterranean deep convection (Ducrocq et al., 2002; Nuissier et al., 2008). The horizontal resolution was 2.4 km grid length. The simulation domain (called D_1 hereafter, Fig. 1) covered an area of about 700 x 700 km^2 centred over the west of Mallorca, and stretching from North Africa to the south of France. In the vertical direction, 40 levels were used, spaced 75 m apart near the ground and up to 900 m apart near the model top. The initial and boundary conditions chosen for this simulation

Fig. 8. ARPEGE analysis at 1200 UTC 4 October 2007: (a) geopotential (red lines, in dagpm) and temperature (shaded, in °C) at 500 hPa, (b) mean sea level pressure (red lines, hPa) and wet bulb potential temperature at 850 hPa (shaded, in °C).

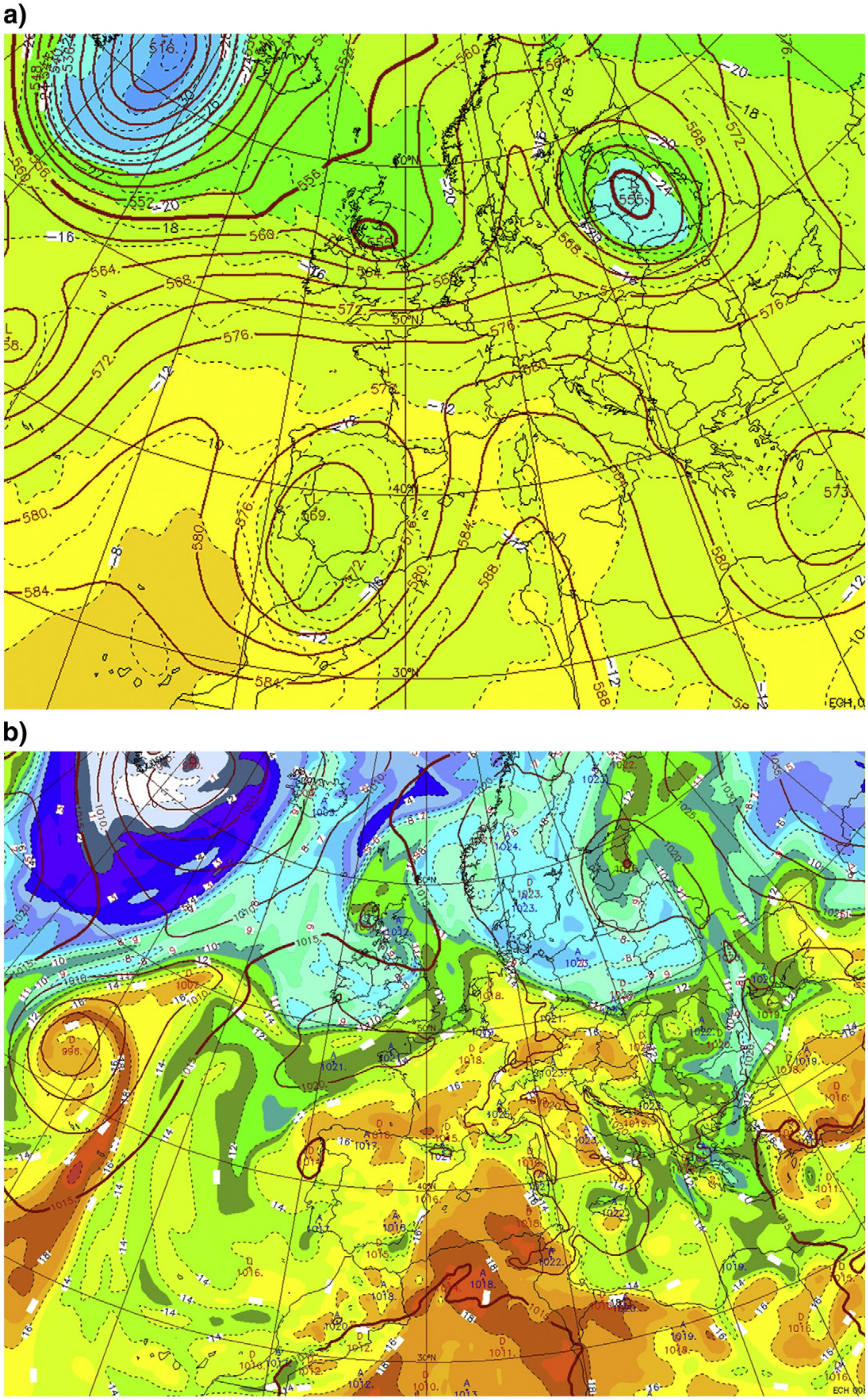
a)
b)

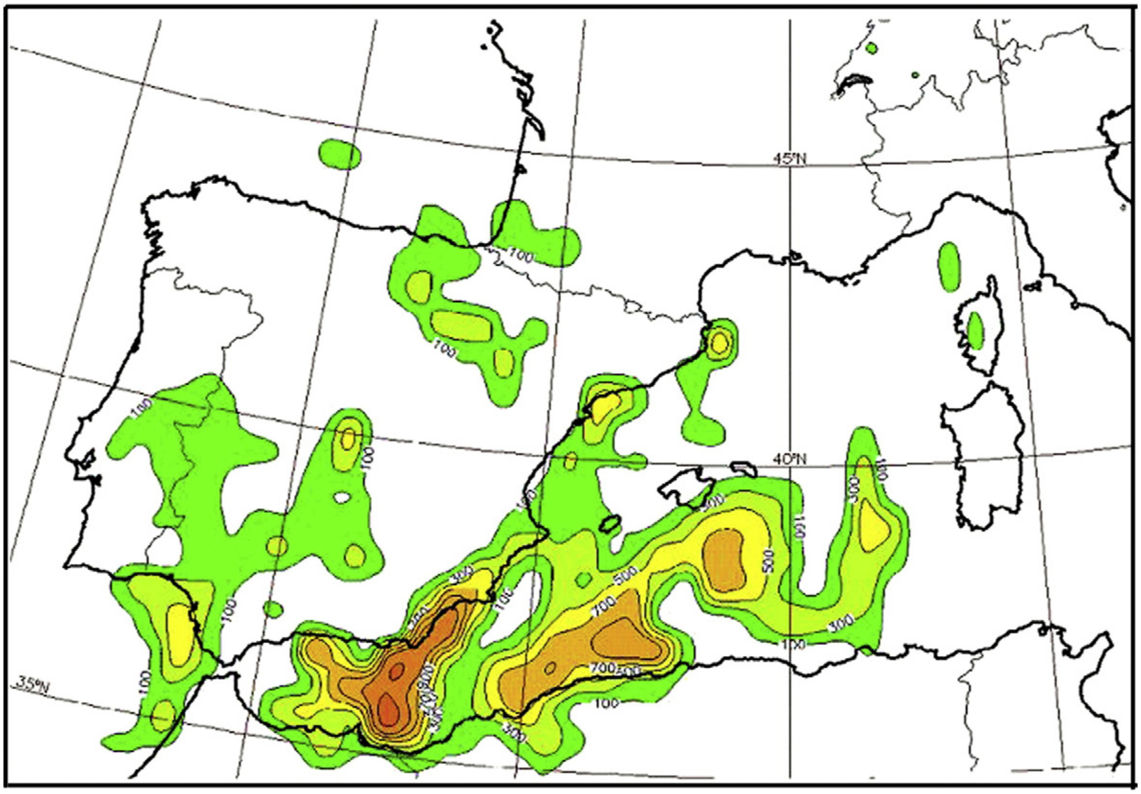

Fig. 9. CAPE on ARPEGE analysis at 0600 UTC on 4 October 2007 for a ground parcel in J kg^{-1}.

were ECMWF analyses provided every 6 h. This simulation started at 0000 UTC and is called $MNH_{2.4}$ hereafter.

4. Results

4.1. Temporal evolution

The main difficulty in evaluating the quality of the simulation was the paucity of available in-situ observations since the event occurred mainly over the sea. In addition, coastal observations indicated a weak and intricate low-level flow, associated with a complex distribution of sea level pressure. Consequently, the main observations used for the validation of the simulation were the remote-sensing ones: weather radar and METEOSAT images. Satellite winds such as those elaborated from the Quickscat scatterometer were not relevant as they are contaminated by rain and only available a few times per day. Fig. 11 displays the simulated reflectivity at 2500 m in $MNH_{2.4}$ superimposed on the wind vectors at 925 hPa at 0900, 1200 and 1500 UTC. A convective system formed offshore of Murcia between 0700 and 0800 UTC in the simulation, which corresponds well with the satellite observations at that time. In contrast, at 0900 UTC, a convective line was simulated along the coast, whereas in the observation, the precipitating system was located to the east, over the Balearic Islands. The triggering of the deep convection offshore of Murcia in the simulation was a response to the low-level convergence, between a well established easterly flow and an area of weaker winds associated with a low centred over Murcia. This area was especially favourable to convection initiation as it was characterized by a warm air tongue at low-levels and cold air aloft. Nevertheless, even though the initial system was initiated at a very satisfactory location in $MNH_{2.4}$, it did not remain stationary for a few hours as observed. The simulated system propagated northeastwards and affected Mallorca at 1300 UTC, i.e. two and a half hours before the observed system. The failure to reproduce the quite stationary evolution of the storm between 0800 and 1100 brought forward to the time when the squall line affected Mallorca. Despite this time difference, the model succeeded very well in simulating the linear convective mode, fed by a perpendicular low-level moist flow. Simulated reflectivities had shapes and locations very close to those observed, although they were 2–3 h in advance (Fig. 11b and c compared to Fig. 7c and d). Both the simulated and observed reflectivities showed an asymmetric pattern with stratiform precipitation located toward the northern edge of the MCS, with the most intense convective cells developing along the southern end of the line. Although the simulated system evolved ahead of the actual storm due to the lack of an initial stationary stage, the remarkable location and orientation of the convective system in this simulation allowed a valuable detailed analysis of the squall line environment and structure to be carried out.

4.2. The MCS environment

The success of $MNH_{2.4}$ in reproducing a convective system close to the observed one allowed us to further explore the MCS environment using this simulation.

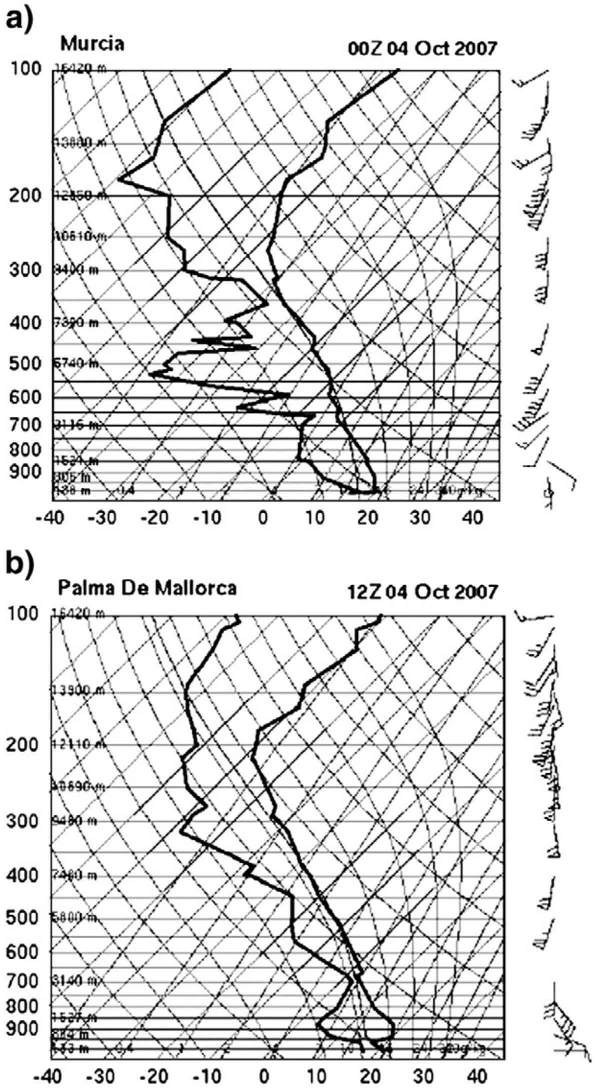

Fig. 10. Soundings on 4 October 2007 from: (a) Murcia at 0000 UTC, and (b), Palma at 1200 UTC.

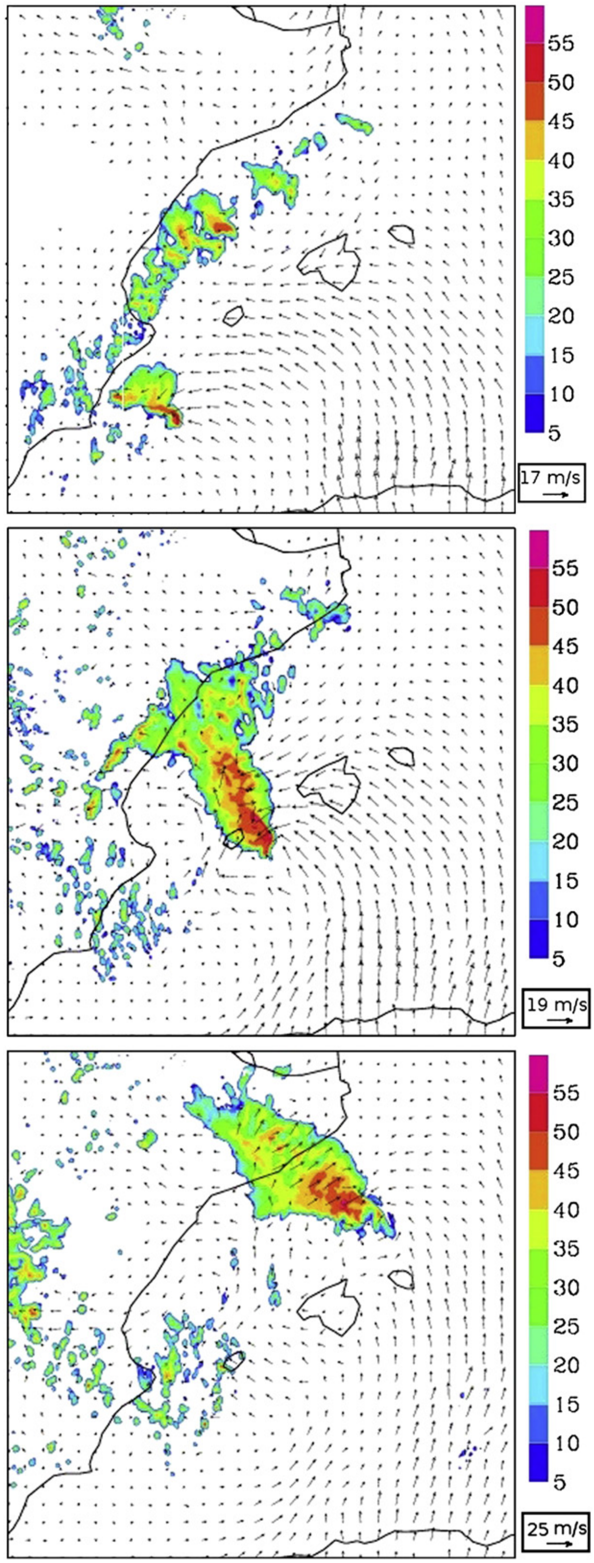

Fig. 11. $MNH_{2.4}$ simulated reflectivity at 2500 m asl (shaded, dBz) and wind at 925 hPa ($m\ s^{-1}$) at 0900 UTC, 1200 UTC and 1500 UTC on domain D_1.

First, the environment was analysed near the initiation time phase when the convective system was being set up offshore of Murcia at 0700 UTC. Associated with the upper-level synoptic forcing, a surface pressure low was centred over northern Africa (Fig. 12a) which induced an easterly flow over the southern Mediterranean that enhanced the low-level lifting along the thermal boundary. This limit was affected by a strong deceleration of the horizontal wind, which implied convergence at low-levels along the front. The Atlas range may have strengthened the low just downstream of the mountains. The easterly flow going along the African coast provided warm, moist air at low-levels which reached the Spanish coast south of Murcia. In the region of the convective initiation, the CAPE was thus rather high (more than 1000 J kg^{-1}, Fig. 12b), and the CIN very weak. Corresponding to the southern part of the low-level convergence line, this region was thus the most propitious for convection initiation

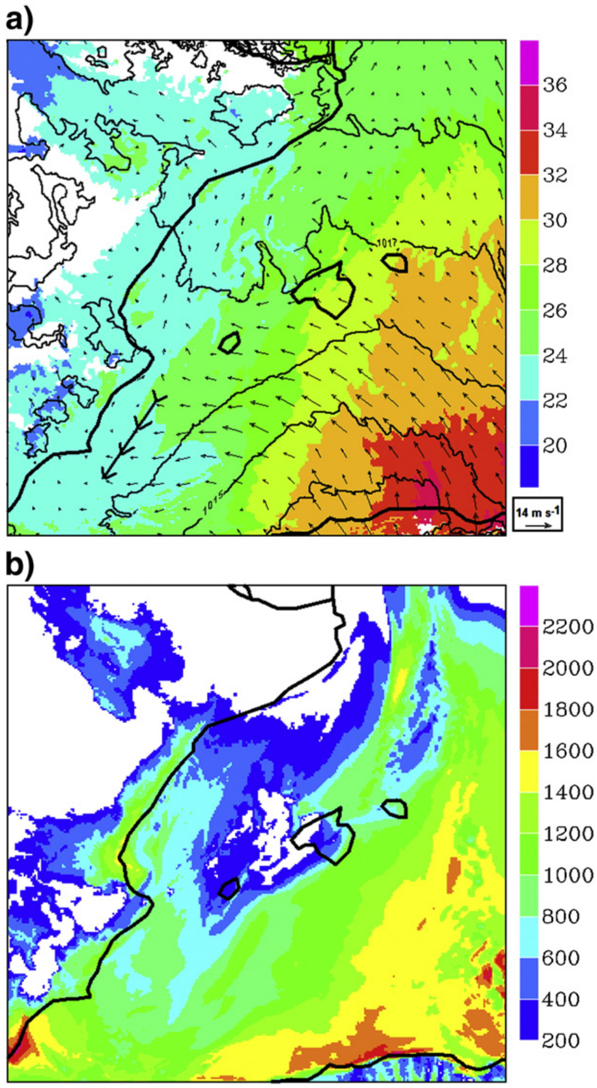

Fig. 12. $MNH_{2.4}$ simulation at 0700 UTC on 4 October 2007; (a): virtual temperature θ_v (shaded, °C) and winds ($m\,s^{-1}$) at 925 hPa and mean sea level pressure (black lines, hPa) on domain D_1, and (b): CAPE maximum (shaded, $J\,kg^{-1}$) on domain D_1.

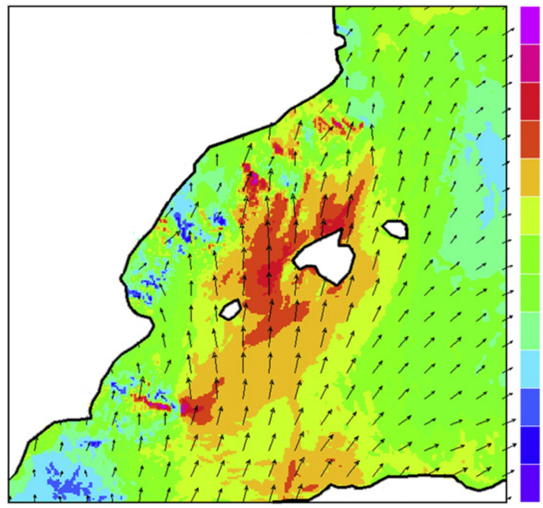

Fig. 13. Horizontal wind shear intensity (shaded, $m\,s^{-1}$) over the sea below 3000 m asl in $MNH_{2.4}$ experiment at 0900 UTC on 4 October 2007 on domain D_1.

(conditionally unstable moist air at low-levels, and lifting) according to the ingredient-based approach of Johns and Doswell (1992). The location of the surface low is thought to have a strong impact on the convective system organization.

After initiation, the convective system evolved along the thermal boundary as shown by the gradient of virtual temperature θ_v at 925 hPa in Fig. 12a. Stationary in its southern part, the warm front moved westwards in the morning and remained rather stationary later, parallel to the Spanish coast, passing through Mallorca. The front was also characterized by a strong shear, especially near the Balearic archipelago as shown in Fig. 13 below 3000 m. Due to the difference between the low-level easterly flow and strong southerly winds aloft, this sheared environment helped to enhance the squall line intensity. Shear values were, on the whole, greater than 15 $m\,s^{-1}$ over the western Mediterranean and shear direction was almost perpendicular to the squall line orientation. Such strong values balanced the vorticity created by the thermal gradient near the gust front and brought about efficient vertical updrafts.

4.3. Squall line internal structure

Because the Méso-NH simulation organizes convection in an asymmetric linear structure very similar to radar observations, this experiment allowed the internal structure of the squall line to be studied. From the sea level pressure fields (Fig. 14a), the classically described characteristics of a squall line are clearly identifiable. Below the rainfall area, as a consequence of cooling by evaporation, a surface high is evidenced as a pressure increase of up to 5 hPa in some places in comparison to the surrounding environment. Ahead of the most active part of the squall line, a pre-squall meso-low is present. The vertical motions show a subsiding flow at mid-levels in front of the convective part (Fig. 14c), which is able to generate a surface low underneath. In addition, under the stratiform part, the wake-low is also well simulated, with a weaker magnitude than the pre-squall meso-low. Thus, pressure characteristics in this experiment are consistent with the squall line conceptual scheme (Houze, 1993) and with observations at the Santa Ponça station (Fig. 4).

Vertical sections completed the analysis of the simulated squall line. The hydrometeor content along the cross section A–B in Fig. 14b points out a multicellular organization proper to squall lines, with cells in different life cycle stages. The mature cells characterized by strong hydrometeor contents in the whole troposphere are the place of updrafts reaching 20 $m\,s^{-1}$ at mid-levels. Due to the southerly flow above 700 hPa, the convective system is asymmetric and the stratiform part is located to the north of the convective one. Old cells with lower hydrometeor contents in are progressively incorporated into the stratiform part as in a multicellular thunderstorm.

The dynamics sustaining the squall line can be understood with the virtual potential temperature (θ_v) cross section

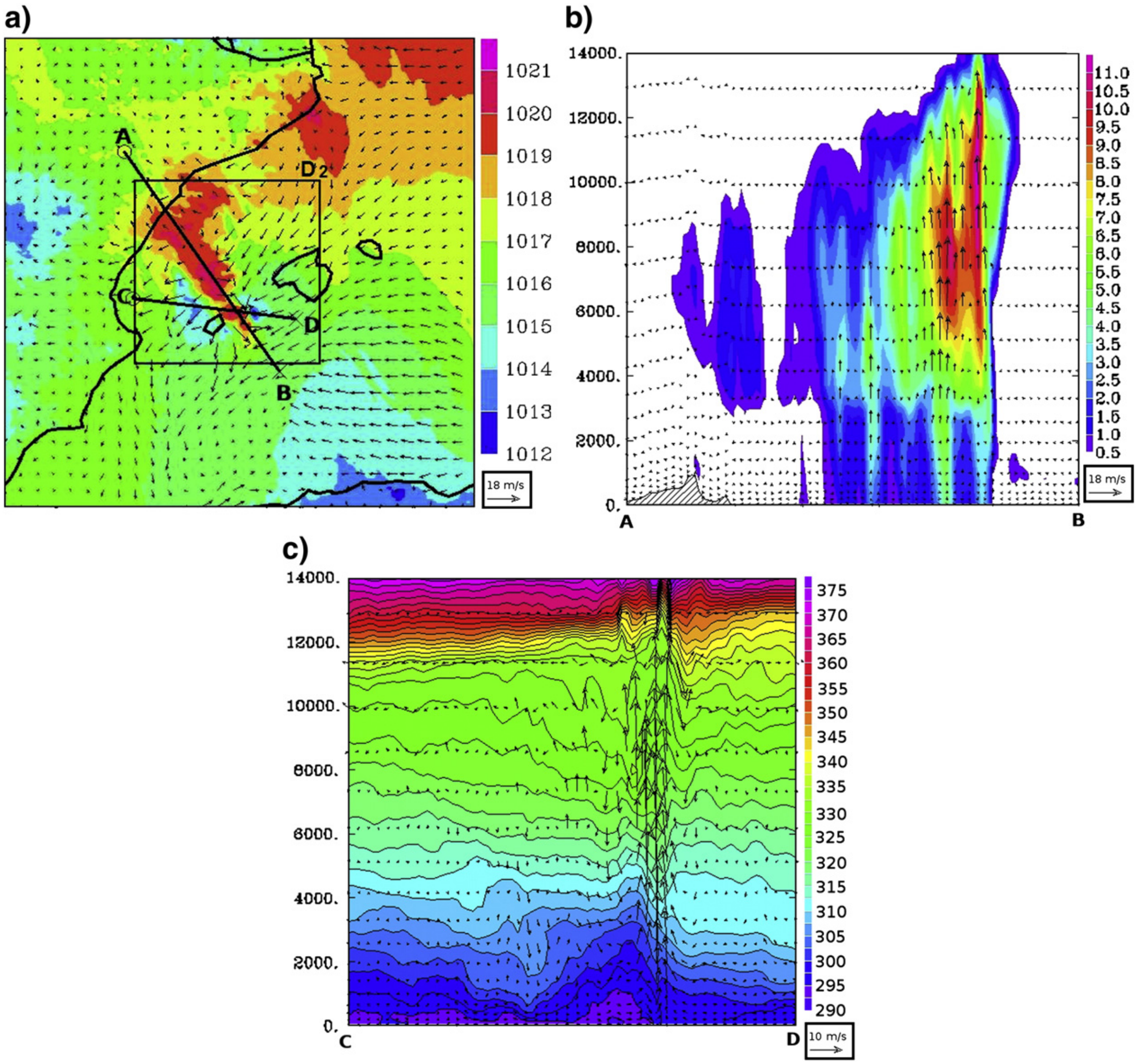

Fig. 14. Squall line features in $MNH_{2.4}$ experiment at 1200 UTC on 4 October 2007; (a): sea level pressure (shaded, hPa) , surface winds (m s^{-1}) on domain D_1, an indication of domain D_2, (b): vertical cross sections of hydrometeor contents (cloud water + rain + ice + snow + graupel, shaded, g kg^{-1}) and vertical motions (m s^{-1}) along the segment A–B, and (c): vertical cross sections of θv (shaded, °K) and vertical motions (m s^{-1}) along the segment C–D. Cross section axes are shown in (a).

displayed in Fig. 14c. The descending rear inflow jet (RIJ) characterized by cold, dry air enhanced by rainfall evaporation is present under the stratiform part. Reaching the surface, this RIJ contributes to the creation of the density current necessary to heighten updrafts in the convective part as a result of low-level convergence. Updrafts are located just ahead of the boundary between the cold pool and the moist environment, where the thermal gradient is high. Therefore, horizontal vorticity generated by the buoyancy gradient is able to balance the opposing vorticity associated with the low-level shear.

Moreover, stratiform region dynamics, physically interpretable with vertical motions (Fig. 14b and c) are in good agreement with the conceptual model of a squall line exposed in Houze (1993). Just at the rear of the convective part, a transition zone of downdrafts is present whereas mesoscale updrafts only appear in a more distant zone of the stratiform part. In addition, downdrafts are associated with precipitation below the stratiform region. Eventually, all the above remarks tend to prove that the simulated MCS shows all the dynamical features that characterize a squall line, but with an asymmetric component.

4.4. Tracking mesovortices

The goal of this section is to determine whether the model that simulates many aspects of the squall line remarkably accurately is also able to produce mesovortices, essential tornado precursors. Admittedly, simulated mesovortices may be very different from the observed ones. However, their development in the simulations is an indication of the presence of supportive environments and dynamics in the actual squall line. The previous simulation with a 2.4 km mesh was not fine enough to track mesovortices, which have diameters of a few kilometres. Therefore, we set up an experiment called $MNH_{0.6}$ with higher resolution, set to 600 m. Due to computational limits, this simulation was performed on a small domain (D_2) and for a short period. Consequently, it was initialized with $MNH_{2.4}$ output, at 1200UTC when the squall line had already formed on $D_{2,}$ a small domain nested in D_1 (Fig. 15a) including the whole squall line. Méso-NH was run for an hour and its boundary conditions were also provided by $MNH_{2.4}$. Physical parameterizations were the same as in $MNH_{2.4}$; thus the only difference was the four-times-higher resolution.

From the beginning of the simulation, a bow echo was conspicuous in radar reflectivities in the southern part of the line. This convective organization was already present in the $MNH_{0.6}$ initial conditions at 1200 UTC, and it remained throughout the simulation, curving progressively. In Fig. 15a, it can be clearly seen that the bow echo has some undulations at locations L_1, L_2 and L_3 on its leading edge and a notable one develops just north of its apex. Near the bow centre, a weak rainfall area must be linked to a strong RIJ, evaporating the precipitation and bending the bow echo (Houze, 1993). Each of these undulations, generated by differences in outflow magnitudes, is an area of enhanced cyclonic vorticity.

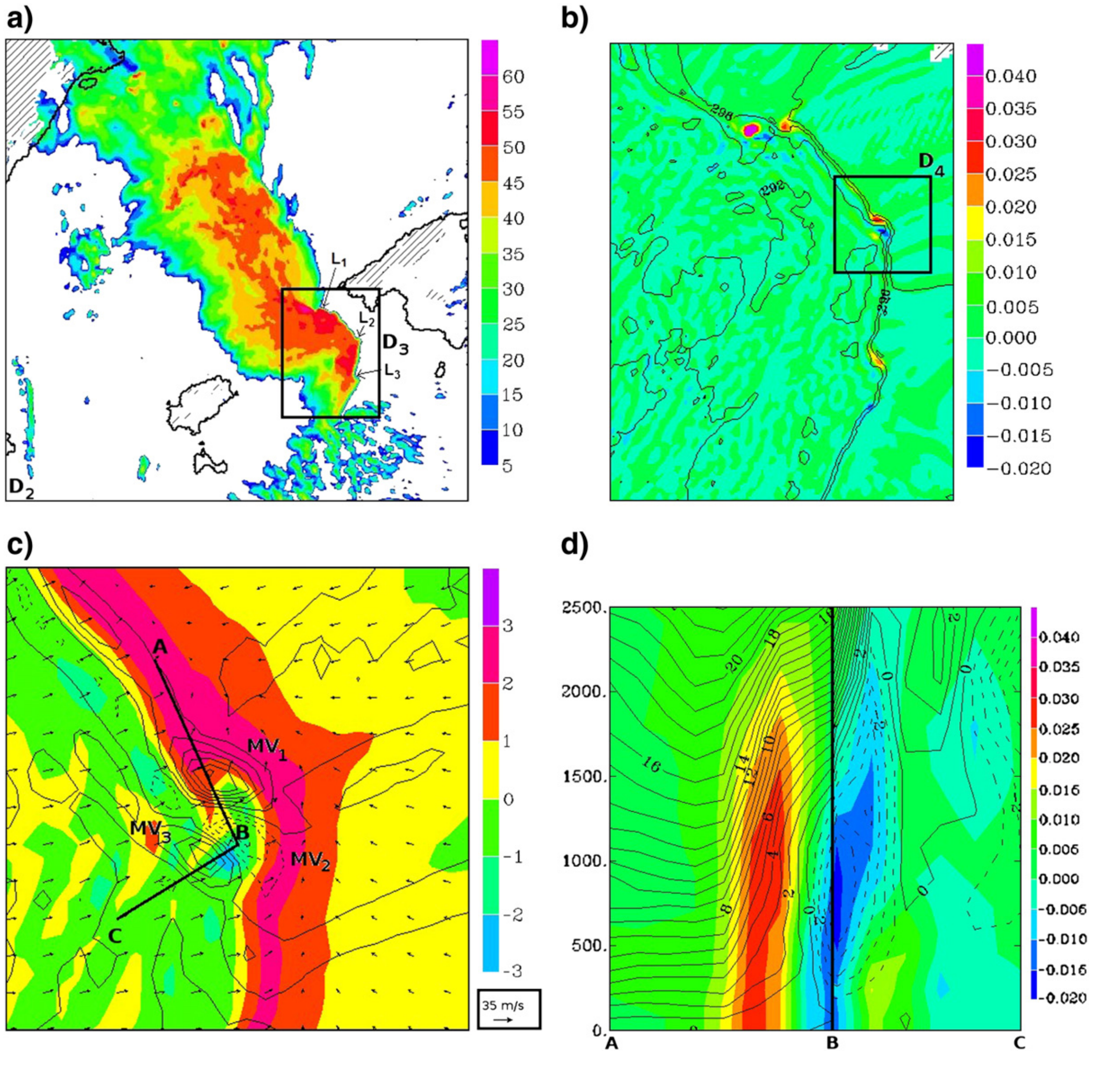

Fig. 15. Very high resolution simulation $MNH_{0.6}$ at 1230 UTC on 4 October 2007 ; (a): reflectivities at 200 m asl on domain D_2 and indication of the domain D_3; (b): vertical vorticity (s^{-1}) at 200 m on domain D_3, θv at 200 m (dark line, every 2 K), and indication of domain D_4; (c): vertical velocities at 200 m on domain D4 (shaded, m s^{-1}), vertical vorticities at 200 m (dark line, negative values in dashed line, every 5.10^{-2} s^{-1}) and wind at 200 m (m s^{-1}); and (d): cross section along the axis A–B–C shown in (c) of vertical vorticity (shaded, s^{-1}) and vertical velocities (black line, negative values in dashed line, every 1 ms^{-1}).

Eventually, this high-resolution simulation shows groups of mesovortices with opposite circulations in three different locations in the bow echo (Fig. 15b), corresponding to three undulations L_1, L_2 and L_3. In particular, the mesovortices are simulated on the cyclonic side of the bow apex.

All the mesovortices in the simulation develop and evolve where the gradient of θ_v is strong (Fig. 15b), and this baroclinically generates tubes of horizontal vorticity. So as to understand the onset of the mesovortices, particular attention was paid to the first positive mesovortex that appeared 20 min into the run near the bow apex. Fig. 16a indicates that the leading edge of the bow echo is characterized by strong updrafts near the ground with a maximum of vertical velocities just at the apex, where the convergence between the RIJ and the eastern flow over Mallorca is strongest. As demonstrated in the recent study by Atkins and St. Laurent (2009a), the most damaging mesovortices are those that develop where the gust front is locally enhanced by a descending RIJ. In contrast, weaker and less damaging winds are produced by mesovortices that develop prior to the RIJ. Fig. 16b clearly shows that the area of maximum updrafts corresponds to the location of the mesovortex that is just developing. In this precise location, the tube of horizontal vorticity visible in blue in Fig. 16b is tilted into vertical vorticity by the strong updrafts. Consequently, in this case, we have good agreement between the formation of a single mesovortex and the mechanism described by Atkins and St. Laurent (2009a). This genesis mechanism considers that the parcels descending within the downdraft acquire horizontal vorticity, which is subsequently tilted by the updraft along the gust front. It is the same mechanism that leads to mesovortices in supercell thunderstorms (Rotunno and Klemp, 1985). These authors also demonstrated that the formation of a single mesovortex is thought to prevail in a strongly sheared environment, and this was confirmed in our simulation.

It is noteworthy that this mesovortex does not stay alone for a long time. At 1230 UTC, a triplet of well defined vortices with opposite circulations evolves near the bow apex (Fig. 15c). They reach a height of 2500 m and their intensity is stronger below 1500 m (Fig. 15d).

The life cycles of such simulated mesovortices are quite short. The variation in the magnitudes of the mesovortices displayed in Fig. 15c are plotted in the graph of Fig. 17. The first mesovortex MV_1 which formed the first has a cyclonic circulation and appears in an updraft area. Later, a couplet of mesovortices (MV_2 and MV_3) is generated with the cyclonic mesovortex to the south. The area between these two mesovortices was affected by downdrafts both at the time presented in Fig. 15c and when they appeared. These relative positions of the two mesovortices prove that the genesis of this couplet of mesovortices matches the classical conceptual scheme proposed by Trapp and Weisman (2003) and evokes a tilting of the horizontal vorticity into vertical vorticity by downdrafts. During the run, other mesovortices of lower magnitude developed to the south to those previously mentioned (MV_4...), and each time with an opposite circulation relative to the mesovortex located to their north. This organization is guaranteed by updrafts between a cyclonic and an anticyclonic mesovortex when the cyclonic one is located to the north and by downdrafts when the cyclonic mesovortex is located to the south. Moreover, other groups of

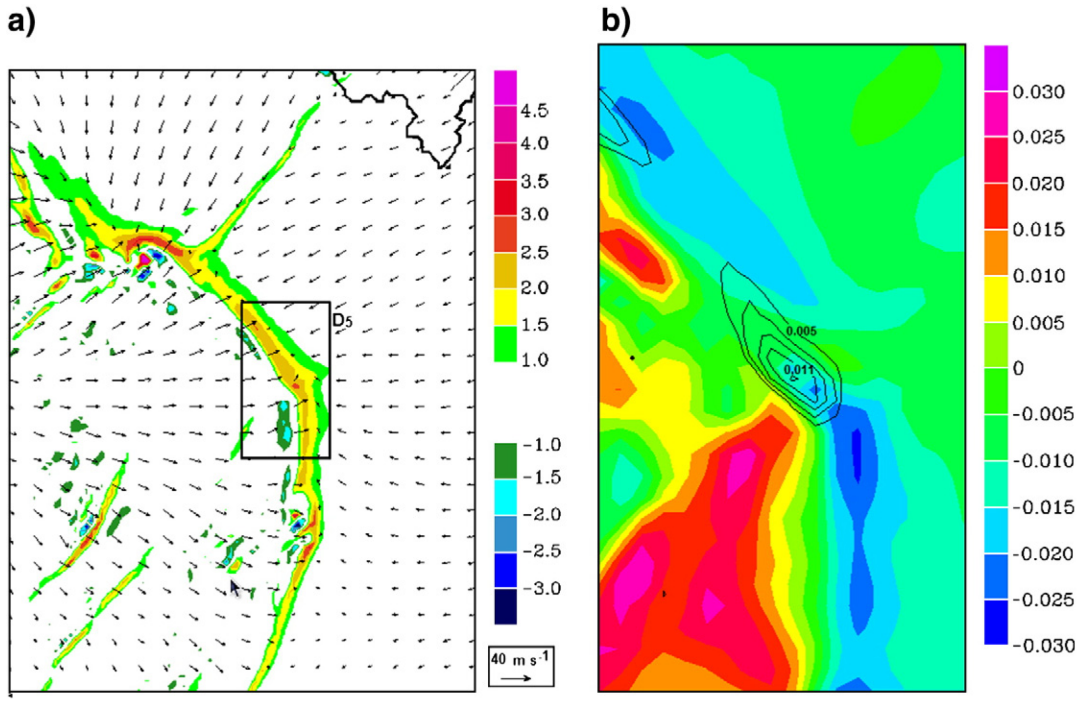

Fig. 16. Simulation $MNH_{0.6}$ at 1220 UTC 4 on October 2007; (a): vertical velocity (shaded, m s^{-1}) and wind (m s^{-1}) at 200 m asl on domain D_3 and indication of the domain D_5; and (b): vertical vorticity (shaded, s^{-1}) and horizontal vorticity along the meridian axis (dark line for positive values up to 5.10^{-3} s^{-1}, every 2.10^{-3} s^{-1}) at 200 m asl on domain D_5.

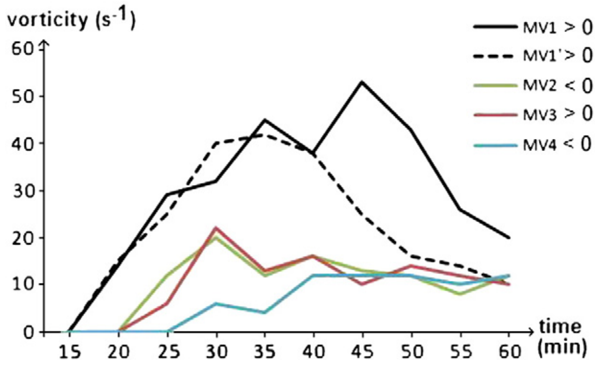

Fig. 17. Bow echo apex mesovortex magnitudes at 200 m asl, for the several mesovortices near the bow apex (lines for MV1, MV2, MV3 and MV4 in $MNH_{0.6}$ simulation, and dashed line for MV1′ in $MNH'_{0.6}$ simulation).

mesovortices visible in the bow echo (Fig. 15b) followed the same kind of evolution with an alternation of mesovortices of opposite circulations.

The presence of these low-level mesovortices in $MNH_{0.6}$ confirms the potential of the severe convective system for the genesis of small-scale vortices, which are essential precursors to tornadoes. In Fig. 7d, it can be seen that the apex of the presumed bow echo is just about to affect the bay of Palma, where tornadoes were observed. Thus, in spite of the time-difference, the experiment $MNH_{0.6}$ reproduced the location of the bow echo with good accuracy.

4.5. Mallorcan orography influence

The prominent orography of Mallorca is hypothesized to have had an influence on the evolution of the mesovortices. We analysed such influence by performing a new simulation called $MNH'_{0.6}$ with a set-up to identical that of $MNH_{0.6}$ but in which the orography of Mallorca was flattened in domain D_2. Admittedly, some influence from the Mallorca orography still remained through the initial and boundary conditions, but differences between simulations could be unequivocally attributed to the direct effect of the mountains. Here, particular attention is paid to the impacts on the group of mesovortices at locations L_1 and L_2.

In $MNH'_{0.6}$, the mesovortices in the leading edge of the squall line begin to weaken before reaching Mallorca. In contrast, the mesovortices obtained in $MNH_{0.6}$ continue to develop while approaching the mountainous island. A quantitative comparison of the simulated mesovortices (Fig. 17) indicates that the mountains in Mallorca contribute to the intensification of MV1 when it is approaching the southwestern coast of the island at 1245 UTC. The reason for this increase is explained in Fig. 18, which presents the vertical vorticity and winds at 200 m at 1245 UTC for the two simulations. The orography of the island induces stronger winds along the corridor between the northern range of mountains and the lower mountains to the south of the island, connecting the bays of Palma and Alcudia. The strong eastern flow collides with the bow echo outflow and creates an area of higher convergence compared to the simulation without orography. The convergence induces a stretching of the vertical tubes of vorticity, and thus an increase in vorticity. The mesovortices of undulation L_1 evolve similarly.

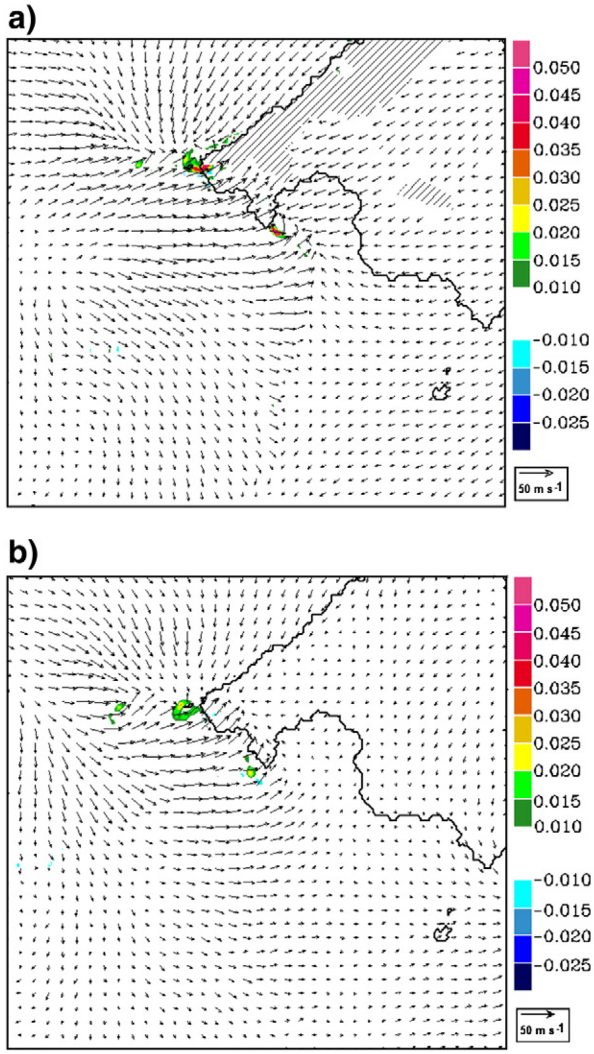

Fig. 18. Vertical vorticity (s^{-1}) and wind at 200 m ($m\ s^{-1}$) at 1245 UTC 4 October 2007; (a): on $MNH_{0.6}$ simulation, and (b): on $MNH'_{0.6}$ simulation (Mallorcan orography removed).

These groups of mesovortices are enhanced by the strong winds impinging on the northern coast of Mallorca whereas mesovortices near the bow apex (L_2) are enhanced by the strong flow coming from inland Mallorca.

Consequently, orographically modified flows are responsible for the reintensification of the mesovortices while approaching the bay of Palma. The comparison of $MNH_{0.6}$ and $MNH'_{0.6}$ proves that the orography of Mallorca is an essential factor for the maintenance and enhancement of the mesovortices. These two simulations allow us to conclude that Palma was an area prone to mesovortex development in this particular case of squall line and this indeed gives clues to explain the location of the tornadoes observed during this severe convective event.

5. Conclusions

The aim of this study was to analyse the severe convective event of 4 October 2007 that affected and strongly damaged the island of Mallorca. An observational study provided clues that the mesoscale convective system responsible was an asymmetric leading line-trailing stratiform system with maritime initiation early in the morning offshore of Murcia. The synoptic situation aloft was characterized by a cut-off over mainland Spain associated with cold air coupled with a southwesterly jet streak and a pronounced positive potential vorticity anomaly. Its effect reached the surface, creating a low pressure area over North Africa and inducing an easterly flow over the southern Mediterranean Sea. This area was also affected by a stationary front separating a moist, warm air mass over the sea from a drier, colder environment from mainland Spain.

The experiment $MNH_{2.4}$ indicated that the MCS initiated and evolved over the thermal boundary. The squall line initiated in an area characterized by a high CAPE and its precise location is explained by a low-level convergence line. The cold and dry layer above the thermal boundary could enhance the precipitation evaporation rate and thus strengthen the squall line rear inflow jet. Moreover, the strongly sheared environment appears to be an important component in the development of a squall line that has large, strong cells.

In this environment, Méso-NH has shown its ability to reproduce a convective linear organization, even though its spatiotemporal evolution is not always well captured. It is rather obvious that higher precision in initial conditions might have allowed better synchrony between simulations and observations. Increased amounts of data from ships in this maritime domain would enable initial conditions of better quality.

However, the multicellular structure associated with the well-identified internal dynamics of a squall line is correctly simulated. The previous experiment containing a bow echo in the southern part of the squall line allowed a very high resolution simulation to be initiated with a grid size of 600 m centred on the convective system. This experiment indicated that mesovortices developed in each undulation of the squall line gust front and in particular near the bow apex. This area affected the bay of Palma both in the simulation and in reality. Such low-level mesovortices confirm the potential of this severe squall line for the genesis of tornadoes.

Although mesovortex formation may be very different between simulated storms and observed ones, our simulation groups together with several mechanism previously identified in numerical studies. The first cyclonic mesovortex formed alone as documented by Atkins and St. Laurent (2009a), after which an alternation of mesovortices characterized by opposite circulations developed to the south. The formation of the first couplet of mesovortex matches the conceptual scheme of Trapp and Weisman (2003) and is caused by downdraft at the leading edge of the cold pool. Consequently, we have evidenced here an original organization of mesovortices combining several processes of formation. A more complete study of mesovortex formation based on a vorticity equation analysis would be an interesting issue for future works.

In addition, an experiment in which Mallorcan orography was removed proved the crucial role played by the orography in heightening mesovortices present on the leading edge of the bow echo due to stronger winds colliding the bow echo outflows. In particular, Palma bay is the place where accelerated winds blow out from a corridor between mountains. As the bow apex arrived just over this area, we found interesting arguments to explain the location where the tornadoes occurred on 4 October 2007.

Acknowledgements

The authors thank Juan Escobar from the Laboratoire d'Aérologie whose help was essential in the successful running of Méso-NH at the UIB. The authors are grateful to Gaëlle Tanguy and Christine Lac for Méso-NH support. Thanks are also due to Regina Guilabert for her software assistance. We thank the Spanish Meteorological Institute AEMET for the data they provided on tornadoes. Sounding pictures were provided by the University of Wyoming. UIB authors also acknowledge support from the MEDICANES/CGL2008-01271/CLI project, granted by the Spanish Ministerio de Ciencia e Innovacion. We also thank Susan Becker for improving the English of the manuscript. Finally, we appreciated the time and effort put in by David Schultz and two anonymous reviewers, whose comments greatly improved the manuscript.

References

Atkins, N.T., St. Laurent, N., 2009a. Bow echo mesovortices, Part I: processes that influence their damaging potential. Mon. Wea. Rev. 137, 1497–1513.

Atkins, N.T., St. Laurent, N., 2009b. Bow echo mesovorticies, Part II: their genesis. Mon. Wea. Rev. 137, 1514–1532.

Betz, H.D., Schmidt, K., Laroche, P., Blanchet, P., Oettinger, W.P., Defer, E., Dziewit, Z., Konarski, J., 2009. LINET — an international lightning detection network in Europe. Atmos. Res. 91, 564–573.

Bougeault, P., Lacarrère, P., 1989. Parameterization of orography-induced turbulence in a meso-beta-scale model. Mon. Wea. Rev. 117, 1870–1888.

Bresson, R., Ricard, D., Ducrocq, V., 2009. Idealized mesoscale numerical study of Mediterranean heavy precipitating convective systems. Meteorol. Atmos. Phys. 103, 45–55.

Bryan, G.H., Knievel, J.C., Parker, M.D., 2005. A multimodel assessment of RKW theory's relevance to squall-line characteristics. Mon. Wea. Rev. 134, 2772–2792.

Buzzi, A., Tartaglione, N., Malguzzi, P., 1998. Numerical simulations of the 1994 Piedmont flood: Role of orography and moist processes. Mon. Wea. Rev. 126, 2369–2383.

Caniaux, G., Redelsperger, J.L., Lafore, J.P., 1994. A numerical study of the stratiform region of a fast-moving squall line. J. Atmos. Sci. 51, 2046–2074.

Colella, P., Woodward, P.R., 1984. The piecewise parabolic method (PPM) for gas dynamical simulations. J. Comput. Phys. 54, 174–201.

Cuxart, J., Bougeault, P., Redelsperger, J.L., 2000. A turbulence scheme allowing for mesoscale and large eddy-simulation. Q. J. R. Meteorol. Soc. 126, 1–30.

Doswell III, C.A., Ramis, C., Romero, R., Alonso, S., 1998. A diagnostic study of three heavy precipitation episodes in the Western Mediterranean region. Weather Forecast. 13, 102–124.

Ducrocq, V., Ricard, D., Lafore, J.P., Orain, F., 2002. Storm-scale numerical rainfall prediction for five precipitating events over France: on the importance of the initial humidity field. Weather Forecast. 17, 1236–1256.

Ducrocq, V., Nuissier, O., Ricard, D., Lebeaupin, C., Thouvenin, T., 2008. A numerical study of three catastrophic precipitating events over Southern France. Part II: mesoscale triggering and stationarity factors. Q. J. R. Meteorol. Soc. 134, 131–145.

Fehlmann, R., Quadri, C., Davies, H.C., 2000. An alpine rainstorm: sensitivity to the mesoscale upper-level structure. Weather Forecast. 15, 4–28.

Homar, V., Stensrud, D.J., 2004. Sensitivities of an intense cyclone over the western Mediterranean. Q. J. R. Meteorol. Soc. 130, 2519–2540.

Homar, V., Ramis, C., Romero, R., Alonso, S., García-Moya, J.A., Alarcón, M., 1999. A case of convection development over the Western Mediterranean sea: a study through numerical simulations. Meterol. Atmos. Phys. 71, 169–188.

Houze, R.A., 1993. Cloud dynamics. International Geophysics Series, 53.

Johns, R.H., Doswell III, C.A., 1992. Severe local storms forecasting. Weather Forecast. 7, 588–612.

Johnson, R.H., 2001. Surface mesohighs and mesolows. Bull. Am. Meteorol. Soc. 82, 13–31.

Khairoutdinov, M.F., Randall, D.A., 2006. High-resolution simulation of shallow-to-deep convection transition over land. J. Atmos. Sci. 63, 3421–3436.
Lafore, J.P., Stein, J., Asencio, N., Bougeault, P., Ducrocq, V., Duron, J., Fischer, C., Hereil, P., Mascart, P., Pinty, J.P., Redelsperger, J.L., Richard, E., Vila-Guerau de Arellano, J., 1998. The Meso-NH atmospheric simulation system. Part I: adiabatic formulation and control simulations. Ann. Geophys. 16, 90–109.
Lebeaupin, C., Ducrocq, V., Giordani, H., 2006. Sensitivity of torrential rain events to the sea surface temperature based on high-resolution numerical forecasts. J. Geophys. Res. 111 (D12), 1211.
Llasat, M.C., Puigcerver, M., 1994. Meteorological factors associated with floods in the North-eastern part of the Iberian Pininsula. Nat. Hazards 9, 81–93.
Massacand, A.C., Wernli, H., Davies, H.C., 1998. Heavy precipitation on the Alpine southside: an upperlevel precursor. Geophys. Res. Lett. 25, 1435–1438.
Montserrat, S., Ramis, C., Thorpe, A., 1991. Large-amplitude pressure oscillations in the western Mediterranean. Geophys. Res. Lett. 18, 183–186.
Nuissier, O., Ducrocq, V., Ricard, D., Lebeaupin, C., Anquetin, S., 2008. A numerical study of three catastrophic precipitating events over southern France. I: Numerical framework and synoptic ingredients. Quart. J. Roy. Meteor. Soc. 134, 111–130.
Nuissier, O., Joly, B., Joly, A., Ducrocq, V., in press. A statistical downscaling to identify the Large Scale Circulation patterns associated with Heavy Precipitation Events over southern France. Q. J. R. Meteorol. Soc.
Pinty, J.P., Jabouille, P., 1998. A mixed-phase cloud parameterization for use in a mesoscale non-hydrostatic model: simulations of a squall line of orographic precipitation. Proc. Conf. Of Cloud Physics, Everett, WA, USA, Amer. Meteor. Soc. Aug. 1999, pp. 217–220.
Ramis, C., Jansa, A., 1983. Condiciones meteorológicas simultáneasa la aparición de oscilaciones del nivel del mar de amplitud extraordinaria en el Mediterráneo occidental. Rev. Geofısica 39, 35–42.
Ramis, C., Arus, J., Lopez, J.L., 1999. Two cases of severe weather in Catalonia (Spain). A diagnostic study. Meteorol. Appl. 6, 11–27.
Ramis, C., Romero, R., Homar, V., 2009. The severe thunderstorm of 4 October 2007 in Mallorca: an observational study. Nat. Hazards Earth Syst. Sci. 9, 1237–1245.
Riosalido, R., 1990. Characterization of mesoscale convective systems by satellite pictures during PREVIMET-89. Segundo Simposio Nacional de Predicción Madrid, Instituto Nacional de Meteorología, pp. 135–148.
Romero, R., Sumner, G., Ramis, C., Genovés, A., 1999. A classification of the atmospheric circulation patterns producing significant daily rainfall in the Spanish Mediterranean area. Int. J. Climatol. 19, 765–785.
Romero, R., Dowell, C.A., Ramis, C., 2000. Mesoscale numerical study of two cases of long-lived quasi-stationary convective systems over eastern Spain. Mon. Wea. Rev. 128, 3731–3751.
Romero, R., Doswell, C.A., Riosalido, R., 2001. Observations and fine-grid simulations of a convective outbreak in northeastern Spain: importance of diurnal forcing and convective cold pools. Mon. Wea. Rev. 129, 2157–2182.
Rotunno, R., Klemp, J.B., 1985. On the rotation and propagation of simulated supercell thunderstorms. J. Atmos. Sci. 42, 271–292.
Scheidereit, M., Schär, C., 2000. Idealised numerical experiments of Alpine Flow regimes and southside precipitation events. Meteorol. Atmos. Phys. 72, 233–250.
Sénési, S.P., Bougeault, P., Chèze, J.L., Cosentino, P., Thepenier, R., 1996. The Vaison-la-Romaine flash flood: mesoscale analysis and predictability issues. Weather Forecast. 11, 417–442.
Tessendorf, S.A., Trapp, R.J., 2000. On the climatological distribution of tornadoes within quasi-linear convective systems. Preprints, 20th Conf. on Severe Local Storms, Orlando, FL, Amer. Meteor. Soc, pp. 134–173.
Trapp, R.J., Davies-Jones, R., 1997. Tornadogenesis with and without a dynamic pipe effect. J. Atmos. Sci. 54, 113–133.
Trapp, R.J., Weisman, M.L., 2003. Low-level mesovortices within squall lines and bow echoes. Part II: their genesis and implications. Mon. Wea. Rev. 131, 2804–2817.
Trapp, R.J., Tessendorf, S.A., Savageau Godfrey, E., Brooks, H.E., 2005. Tornadoes from squall lines and bow echoes. Part I: climatological distribution. Weather Forecast. 20, 23–34.
Wakimoto, R.M., Murphy, H.V., Davis, C.A., Atkins, N.T., 2006. High winds generated by bow echoes. Part II: the relationship between the mesovortices and damaging straight-lines winds. Mon. Wea. Rev. 134, 2813–2829.
Weisman, M.L., Trapp, R.J., 2003. Low-level mesovortices within squall lines and bow echoes. Part I: overview and dependence on environmental shear. Mon. Wea. Rev. 131, 2779–2803.
Wheatley, D.M., Trapp, R.J., 2008. The effect of mesoscale heterogeneity on the genesis and structure of mesovortices within quasi-linear convective systems. Mon. Wea. Rev. 136, 4220–4241.